Anchoring Hydrous RuO_2 on Graphene Sheets for High-Performance Electrochemical Capacitors

By *Zhong-Shuai Wu, Da-Wei Wang, Wencai Ren,* Jinping Zhao, Guangmin Zhou, Feng Li,* and *Hui-Ming Cheng**

Hydrous ruthenium oxide (RuO_2)/graphene sheet composites (ROGSCs) with different loadings of Ru are prepared by combining sol–gel and low-temperature annealing processes. The graphene sheets (GSs) are well-separated by fine RuO_2 particles (5–20 nm) and, simultaneously, the RuO_2 particles are anchored by the richly oxygen-containing functional groups of reduced, chemically exfoliated GSs onto their surface. Benefits from the combined advantages of GSs and RuO_2 in such a unique structure are that the ROGSC-based supercapacitors exhibit high specific capacitance (~570 F g^{-1} for 38.3 wt% Ru loading), enhanced rate capability, excellent electrochemical stability (~97.9% retention after 1000 cycles), and high energy density (20.1 Wh kg^{-1}) at low operation rate (100 mA g^{-1}) or high power density (10000 W kg^{-1}) at a reasonable energy density (4.3 Wh kg^{-1}). Interestingly, the total specific capacitance of ROGSCs is higher than the sum of specific capacitances of pure GSs and pure RuO_2 in their relative ratios, which is indicative of a positive synergistic effect of GSs and RuO_2 on the improvement of electrochemical performance. These findings demonstrate the importance and great potential of graphene-based composites in the development of high-performance energy-storage systems.

1. Introduction

Electrochemical capacitors (ECs) have emerged with great potential to provide energy density higher by orders of magnitude than conventional capacitors, and greater power density and longer cycling life than batteries through the use of high-surface-area electrodes and fast surface-charge-storage processes, which bridge the gap between conventional capacitors and batteries.[1–5] So far, three main kinds of materials; carbon materials, conducting polymers, and metal oxides, have been proposed and independently or collaboratively applied in carbon-based electrochemical double-layer capacitors (EDLCs),[6–8] polymer-, metal oxide-based pseudocapacitors,[9–11] and hybrid supercapacitors.[12–15]

Graphene,[16–18] a unique two-dimensional carbon material, is predicted to be an excellent electrode material candidate for energy-conversion/storage systems because of its high specific surface area, good chemical stability, and excellent electrical and thermal conductivity as well as remarkably high mechanical strength and Young's modulus. Recent progress in large-scale synthesis of graphene sheets (GSs)[19–22] has promoted extensive exploration of graphene-based supercapacitors.[23–28] For example, M. D. Stoller et al. demonstrated the exciting potential of chemically modified graphene for ECs with specific capacitances of 135 F g^{-1} and 99 F g^{-1} in aqueous KOH and organic electrolytes, respectively.[24] However, GSs usually suffer from serious agglomeration and restacking during utilization as an electrode material due to the van der Waals interactions between neighboring sheets, which lead to a great loss of effective surface area and consequently a lower capacitance than as expected. Therefore, keeping the GSs separated within the electrodes may be an effective way to enhance the electrochemical performance of GS-based supercapacitors.

As a typical electrode material used in metal-oxide-based supercapacitors, ruthenium oxide (RuO_2), especially hydrous and amorphous RuO_2, has a high capacitance, reversible charge–discharge features, and good electrical conductivity, all of which make it the focus of research and development of supercapacitors with great potential for achieving higher energy and power densities than carbon-based EDLCs and polymer-based pseudocapacitors, despite its high cost. Moreover, the formation and good dispersion of fine amorphous hydrous RuO_2 particles are of importance to further improve the pseudocapacitive capacitance of the RuO_2 electrode.[29,30] However, RuO_2 particles often tend to form big agglomerates, which may significantly degrade their electrochemical performance due to incomplete reaction of RuO_2 during the electrochemical redox process that starts from the surface of RuO_2 particles and becomes slower as the reaction proceeds, especially for agglomerated large particles.[31] In order to utilize both Faradaic and non-Faradaic processes for

[*] Z.-S. Wu, Dr. W. Ren, J. Zhao, G. Zhou, Dr. F. Li, Prof. H.-M. Cheng
Shenyang National Laboratory for Materials Science
Institute of Metal Research
Chinese Academy of Sciences
72 Wenhua Road, Shenyang 110016, P. R. China
E-mail: wcren@imr.ac.cn; cheng@imr.ac.cn
Dr. D.-W. Wang
ARC Centre of Excellence for Functional Nanomaterials, AIBN
The University of Queensland
Brisbane 4072, Australia

DOI: 10.1002/adfm.201001054

large capacity-charge storage, various RuO_2/carbon composites, such as mesoporous carbon,[31,32] activated carbon,[33,34] carbon nanotubes,[30,35–38] exfoliated graphite,[39] and carbon paper,[40] were explored as electrode materials for hybrid supercapacitors with enhanced energy-storage capabilities and lower cost. However, the electrochemical performance of most porous carbon-based electrodes is limited by the surface area blocked by loaded RuO_2 particles that may not be accessible by the electrolyte used; therefore the advantages of high-surface-area carbon-based double-layer capacitance can not be fully utilized in these composites.

Graphene ensembles have a flexible porous structure due to the intrinsic two-dimensional nature of graphene. Moreover, GSs obtained by reduction of chemically exfoliated graphene oxide are rich in oxygen-containing functional groups, which allows the formation and uniform anchoring of fine nanomaterials via strong chemical interactions between the functional groups of graphene and the nanomaterials.[41] As a result, RuO_2/GSs composites may perform much better than other RuO_2/carbon composites in terms of the absence of pore blockage during the RuO_2-loading process and the anchoring of fine RuO_2 particles uniformly on the surface of conducting GSs. At the same time, the loading of fine RuO_2 particles can avoid or decrease the possibility of serious agglomeration and restacking of GS ensembles, and consequently provide a higher available electrochemically active surface area for increasing EDLC energy storage, owing to the spacing effect of RuO_2 particles between neighboring GSs. Therefore, a high electrochemical performance can be expected for amorphous hydrous RuO_2 nanoparticle (NP)/GS composite electrodes by exploiting the full advantages of graphene-based double-layer capacitance and RuO_2 pseudocapacitance.

In the present work, hydrous RuO_2/GS composites (ROGSCs) with different loadings of Ru for high-performance ECs were prepared by combining a sol-gel process and low-temperature annealing. The amorphous hydrous RuO_2 particles attach onto the surface of the graphene and serve as spacers to support adjacent GSs, which facilitates the electron transfer from graphene to the RuO_2 particles and builds up expanded ionic highways for hydrated protons to access the active surfaces of the ROGSC electrode. The specific capacitance of ROGSC-based supercapacitors shows a monotonic increment with increasing Ru content. A maximum specific capacitance of 570 F g^{-1} is obtained for ROGSCs with 38.3 wt% Ru, which is much higher than that of the pure GSs (148 F g^{-1}). In addition, the ROGSC-based supercapacitors exhibit enhanced rate capability, excellent electrochemical stability, and high energy/power density. The above excellent electrochemical performance of ROGSCs is suggested to be attributed to their unique particle–sheet structure with an enlarged surface area, flexible conductive graphene network, and well-dispersed fine particles for effective charge access and propagation.

2. Results and Discussion

2.1. Synthesis of ROGSCs

Graphene sheets (≤3 layers) were prepared as described elsewhere,[42] by chemical exfoliation of natural graphite powder (500 mesh), in which most of the individual GSs are stacked and aggregated together after the removal of solvent (**Figure 1a**). As we mentioned above, such aggregated GSs dramatically reduce the electrochemically active surfaces available for supercapacitor applications. To obtain high-performance supercapacitors, ROGSCs were fabricated by combining a sol-gel process and low-temperature annealing, as illustrated in Figure 1. In general, the solvent-free GSs were first redispersed in a mixed solvent of ethanol and water, which lead to the release of the stacked sheets to give well-separated individual sheets (Figure 1b). The presence of well-separated individual GSs is a precondition for loading RuO_2 particles anchored onto their planes during the sol-gel process (Figure 1c), and the presence of water offers an aqueous medium (NaOH) for the formation of ruthenium hydroxide. Then ruthenium hydroxide NPs, the precursors of hydrous RuO_2 NPs, were formed by the reaction of $RuCl_3$ and NaOH, and anchored onto the surface of the GSs by strong chemical interactions between the residual oxygen-containing functional groups on the GSs and ruthenium hydroxide NPs, or by van der Waals interactions between the GSs and the NPs.[41,43] Finally, annealing was carried out at 150 °C to convert ruthenium hydroxide NPs into hydrous and amorphous rather than crystalline RuO_2 NPs, to further improve the electrochemical capacitance of the ROGSCs (Figure 1d).[9] The attachment of ruthenium hydroxide NPs onto the GSs effectively prevents the agglomeration of the GSs during the annealing process, which leads to the formation of well-dispersed fine RuO_2 NPs. The in situ formed RuO_2 particles can serve as spacers to prevent aggregation of individual GSs, and form a particle–sheet structured RuO_2/GSs composite. It is reasonable to expect that such in situ formed ROGSCs have a richer porous structure and larger available surface area for the charge-storage/delivery process than those obtained by direct mixing of solvent-free GSs and RuO_2.

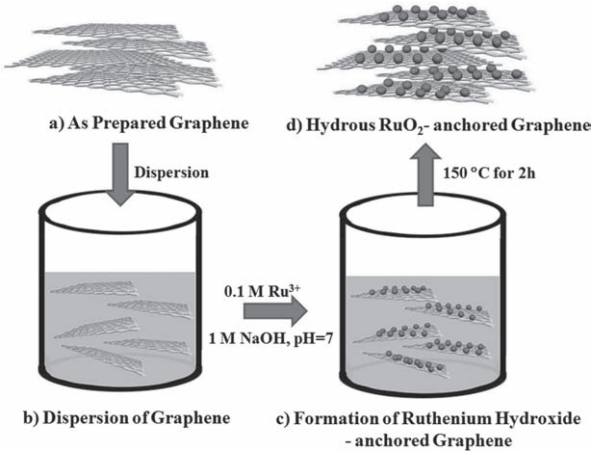

Figure 1. The preparation of ROGSCs by combining a sol-gel method and low-temperature annealing.

2.2. Physicochemical Properties of ROGSCs

The structure and morphology of the ROGSCs were investigated by X-ray diffraction (XRD), thermogravimetric analysis/

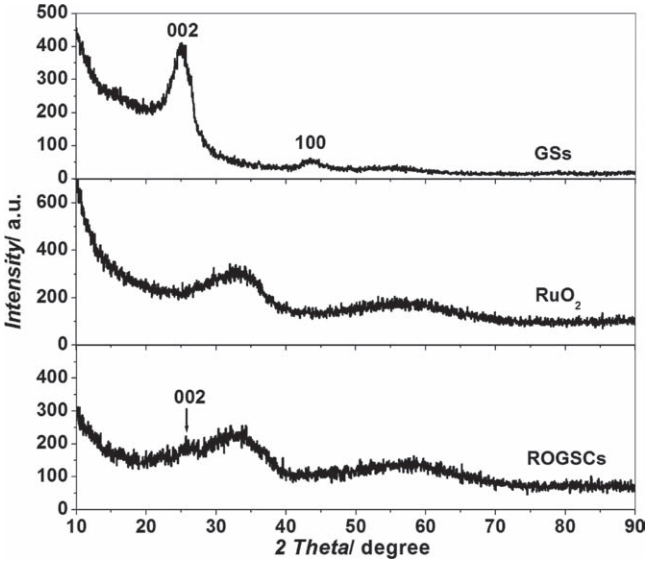

Figure 2. Powder XRD patterns of the as-prepared GSs, RuO_2, and ROGSCs with 38.3 wt% Ru.

differential thermogravimetry (TGA/DTG), X-ray photoelectron spectroscopy (XPS), Raman spectroscopy, liquid-nitrogen cryosorption, scanning electron microscopy (SEM) equipped with energy dispersive spectroscopy (EDS), and transmission electron microscopy (TEM). **Figure 2** shows the XRD profiles of as-prepared GSs by chemical exfoliation, RuO_2, and in situ formed ROGSCs with 38.3 wt% Ru. The loading of Ru in the ROGSCs was determined by using EDS. The low and broad (002) and (100) diffraction peaks observed from the as-prepared GSs illustrate the disordered stacking of GSs.[44] For ROGSCs, the (002) diffraction peak corresponding to the as-prepared GSs almost disappears and no crystalline RuO_2 diffraction peaks are observed, as they are for the pure RuO_2 particles. This result reveals that the GSs in ROGSCs are well separated and the RuO_2 is amorphous due to the low annealing temperature of 150 °C.[29] To further confirm the composition of RuO_2 components in ROGSCs, we performed TGA/DTG measurements on pure RuO_2 prepared with the same conditions as those for the preparation of ROGSCs, but in the absence of GSs (**Figure 3**). The use of pure RuO_2 avoids the influence of GSs on the determination of the RuO_2 content in ROGSCs. The total weight loss, which occurred continuously from 30 °C to 800 °C, is about 17.13 wt%, and the weight loss observed at 133 °C and 235 °C from the DTG curve is attributed to the loss of chemisorbed and crystalline water, respectively. Based on these results, we suggest that the RuO_2 component in ROGSCs has a composition of $RuO_2 \cdot 1.53H_2O$ (Ru, 62.9 wt%). The much slower weight loss observed between 250 °C and 600 °C from the TGA curve further proves that the RuO_2 in ROGSCs is amorphous rather than crystalline.[9,29]

Figure 4 shows the comparative XPS results of the as-prepared GSs and ROGSCs with 38.3 wt% Ru. For the as-prepared GSs, the C1s (284.6 eV) peak is clearly observed; this peak corresponds to the graphitic carbon atoms in graphene.[21] In the spectra of the ROGSCs, many distinct Ru XPS signals such as 3s, 3p, 3d, 4s, and 4p appear in addition to the C1s and O1s

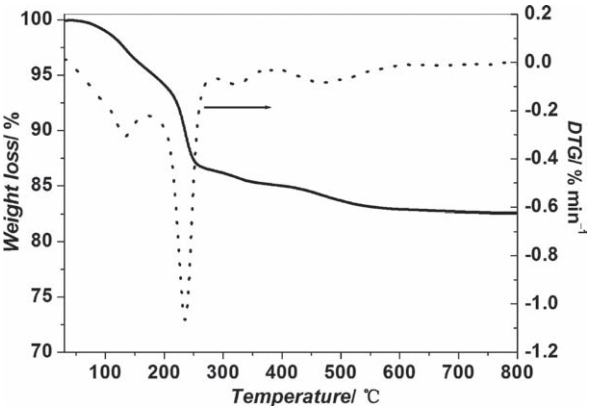

Figure 3. TGA/DTG curves of RuO_2 prepared with the same conditions as those for the preparation of ROGSCs, but in the absence of GSs.

(~529 – 534 eV) signals corresponding to O–C bonds in graphene and O–Ru bonds in RuO_2. Moreover, the Ru $3d_{5/2}$ peak, which does not overlap with Ru $3d_{3/2}$ and $C1_S$ peaks, appears at 281.0 eV; this corresponds to the binding energy of Ru^{4+} and suggests the presence of RuO_2 in the composites.[30] **Figure 5** shows the Raman spectra of hydrous RuO_2 and the as-prepared GSs and ROGSCs with 38.3 wt% Ru. The spectrum of the hydrous RuO_2 with an amorphous structure shows three distinct peaks located at ~513, 625, and 692 cm^{-1},[45] and that of the GSs shows a D band at ~1330 cm^{-1} and a G band at ~1590 cm^{-1}.[46] It is worth noting that both the characteristic peaks of the GSs and of hydrous RuO_2 are observed in ROGSCs. The XPS and Raman results further suggest the good integration of hydrous RuO_2 and GSs.

The nitrogen-adsorption and -desorption isotherms of the as-prepared GSs and ROGSCs exhibit type IV characteristics (**Figure 6a**), which are indicative of the presence of relatively large pores in the samples. It is worth noting that the Brunauer–Emmett–Teller (BET) specific surface area of ROGSCs with 38.3 wt% Ru (281 $m^2\ g^{-1}$) is much higher than that of GSs (108 $m^2\ g^{-1}$) and of pure RuO_2 powder (3.0 $m^2\ g^{-1}$, Figure S1 in Supporting Information). This result strongly suggests that the

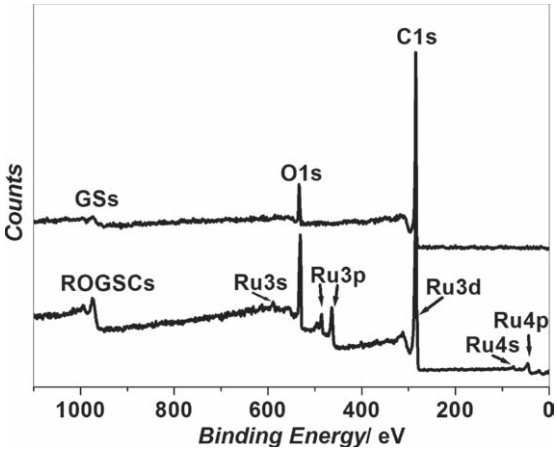

Figure 4. XPS spectra of the as-prepared GSs and ROGSCs with 38.3 wt% Ru.

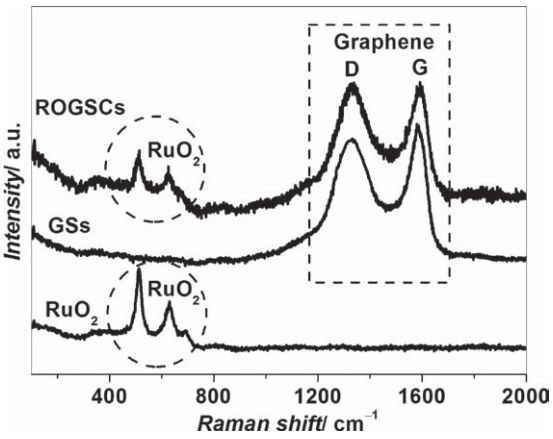

Figure 5. Raman spectra of hydrous RuO_2, as-prepared GSs, and ROGSCs with 38.3 wt% Ru. The dotted circles indicate the characteristic Raman peaks of hydrous RuO_2, and the dotted square frame indicates the characteristic Raman peaks of GSs.

RuO_2 NPs anchored on the separated graphene surface prevent the GSs from aggregating and restacking after the removal of solvents, which finally leads to a porous structure of ROGSC powder with a high specific surface area,[47] as illustrated in Figure 1. Based on the density-functional-theory (DFT) model, the as-prepared GSs and ROGSCs have similar pore-size distributions, from micropores to macropores (Figure 6b), which are different from that of RuO_2 powder (Figure S1). Importantly, an apparent increment in pore volume was observed from 0.325 $cm^3\ g^{-1}$ for as-prepared GSs to 0.366 $cm^3\ g^{-1}$ for ROGSCs, which further indicates the separation of GSs induced by the loading of RuO_2 NPs.

To further characterize the structure of the ROGSCs, we performed TEM and SEM studies (**Figure 7**). For comparison, we also present the TEM images of reduced chemically exfoliated GSs (Figure 7a), NPs formed on the surface of graphene oxide and chemical vapor deposition grown graphene (Figure S2), and SEM images of as-prepared GSs (Figure 7c) and RuO_2 obtained without the presence of chemically exfoliated GSs (Figure S3). Figure 7a shows that solvent-dispersed GSs are almost transparent with some wrinkles visible under TEM. Many small RuO_2 NPs of 5 to 20 nm in size are homogeneously anchored onto the surface of the GSs in the ROGSCs (Figure 7b). As a sharp contrast, without the presence of GSs, the as-prepared hydrous RuO_2 powder tends to spontaneously agglomerate and form big particles with a size of hundreds of nanometers or even tens of micrometers (Figure S3). Further comparisons suggest that the presence of oxygen-containing functional groups on the surface of the chemically derived GSs plays an essential role in anchoring and formation of fine RuO_2 NPs (Figure 7b, Figure S2). Considering that sonication was used during the preparation of TEM specimens, the above observations also demonstrate the strong interactions between NPs and GSs. In the case of a higher loading of Ru species, the number of RuO_2 particles on the GS surface increases and a slight agglomeration is observed. The SEM images also clearly show the difference between the as-prepared GSs and ROGSCs. The as-prepared GSs tend to be randomly distributed and restacked (Figure 7c). However, in ROGSCs, the small RuO_2 particles are highly dispersed on the surface of the GSs and served as spacers to prevent the GSs from restacking (Figure 7d), which is consistent with the increased surface area of ROGSCs over the as-prepared GSs.

From the above results, the structural characteristics of ROGSCs can be summarized as follows: i) The sol-gel process and low-temperature annealing allow for the formation of fine amorphous hydrous RuO_2 on the surface of GSs with the help of oxygen-containing functional groups; this material can display higher electrochemical capacitance than that of the crystalline form.[9] ii) The particle-attached, layered structure of ROGSCs has a highly effective surface-area contact with the electrolyte and a rich porous structure due to the spacing effect of RuO_2 particles between adjacent GSs (conductive backbone), which makes the conduction paths for protons easily accessible to even the inner part of adjacent GSs in the ROGSCs. iii) The adjacent GSs with uniformly anchored RuO_2 NPs can bridge one another, which facilitates the electron transfer from GSs to RuO_2 particles and builds up ionic highways for hydrated protons to access the active surfaces of the ROGSC electrode. Therefore, such structural features ensure the effective utilization of both RuO_2 and GSs in composite electrodes.

2.3. Electrochemical Behavior of GSs and ROGSCs

2.3.1 Cyclic Voltammetry of GSs and ROGSCs

Cyclic voltammetry (CV) was carried out to study the electrochemical capacitive performances of the as-prepared GSs, RuO_2,

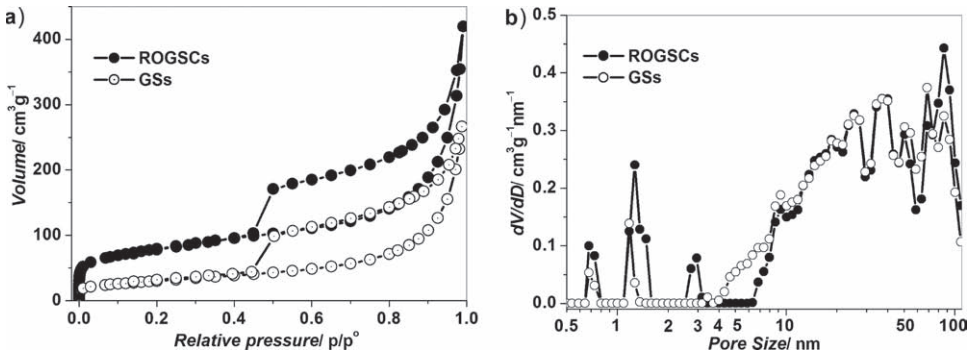

Figure 6. a) Nitrogen-adsorption and -desorption isotherms, and b) pore-size distribution of the as-prepared GSs and ROGSCs with 38.3 wt% Ru.

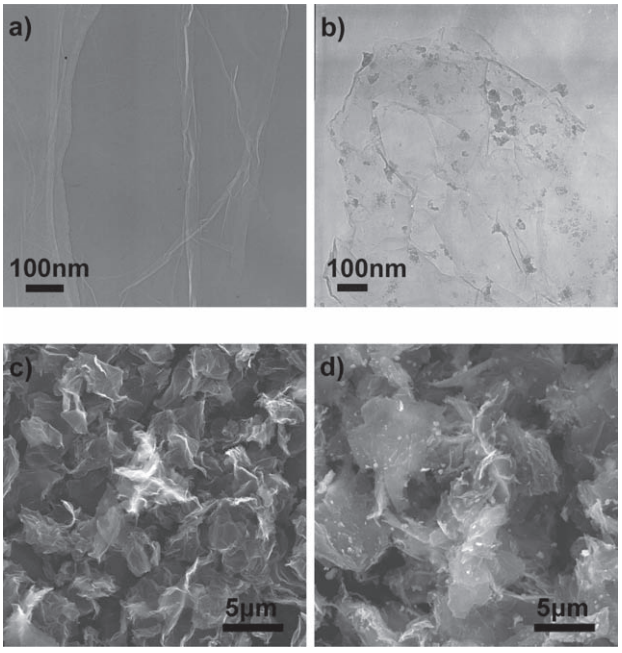

Figure 7. a, b) TEM and c, d) SEM images of the as-prepared GSs (a, c) and ROGSCs (b,d) with 38.3 wt% Ru.

and ROGSC electrodes. **Figure 8** shows the CV results of GSs, RuO_2, and ROGSC (Ru, 38.3 wt%) electrodes, which were measured in 1 M H_2SO_4 at potential intervals from –0.2 – 0.8 V vs. saturated calomel electrode (SCE). The CV curve of GSs in Figure 8a is almost featureless (rectangular box shaped) in the potential window of –0.2 – 0.8 V vs. SCE and the capacitive current density increases with increasing potential scan rate. This result indicates that the GS electrode exhibits typical electrochemical double-layer capacitive behavior that is highly reversible. In a significant difference from the GS electrode, both the RuO_2 and ROGSC electrodes exhibit very broad redox peaks in the investigated potential region, which is indicative of a typical pseudocapacitive behavior of RuO_2 (Figure 8a). The larger voltammetric current for ROGSCs mainly comes from the pseudocapacitance of RuO_2 and partially from electric-double-layer capacitance of GSs (Figure 8a). The specific capacitance (C_{sp}) from the voltammetric response was calculated based on the following equation,[31] $C_{sp} = \frac{1}{mv(V_f - V_i)} \int_{V_i}^{V_f} I(V)dV$, where m is the mass of the active electrode material, v is the scan rate, V_f and V_i are the integration potential limits of the voltammetric curve, and $I(V)$ is the voltammetric current. The specific capacitances of pure GS, RuO_2, and ROGSC electrodes obtained at 1 mV s^{-1} are 148 F g^{-1}, 606 F g^{-1}, and 570 F g^{-1}, respectively (Figure 8b). It is worth noting that the specific capacitance of the ROGSC electrode is much larger than that of the GS electrode at the same scan rate. Compared to pure RuO_2, the ROGSC electrode not only exhibits higher specific capacitance at high rates of between 20 – 50 mV s^{-1}, but also presents better rate capability (47%, 36% for pure RuO_2; Figure 8b). These results imply that the electrochemical Faradaic reactions of fine RuO_2 in ROGSC materials are responsible for the great enhancement of capacitance of the ROGSC electrode, and GSs in ROGCSs are responsible for the improvement of specific capacitance at high rates and high rate capability.

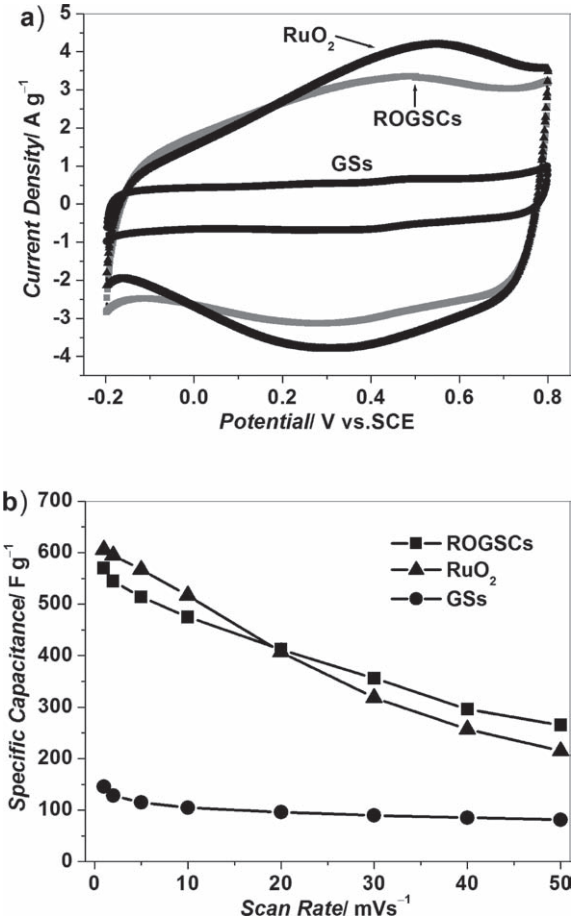

Figure 8. a) CV curves of the as-prepared GS, RuO_2, and ROGSC (Ru, 38.3 wt%) electrodes measured at 5 mV s^{-1} at potential intervals from –0.2 to 0.8 V vs. SCE in 1 M H_2SO_4. b) The C_{sp} of the as-prepared GS, RuO_2, and ROGSC (Ru, 38.3 wt%) electrodes as a function of scan rate.

2.3.2 Effect of Ru Loading of ROGSCs on ECs

In order to further understand the effect of Ru content on the electrochemical performance of the ROGSC electrode, ROGSCs with different Ru-loadings of 6.7, 14.7, 31.5, and 38.3 wt% were prepared. **Figure 9a** shows the typical CV curves of ROGSC electrodes measured in 1 M H_2SO_4 at a low scan rate (1 mV s^{-1}) between –0.2 and 0.8 V vs. SCE. A gradual change of capacitive behavior is observed from rectangular-shaped CV profiles related to EDLC behavior at low loading of Ru (6.7 and 14.7 wt%) to the RuO_2 pseudocapacitive characteristics at high loading of Ru (31.5 and 38.3 wt%). Moreover, the integrated areas under the CV curves increase with decreasing GS content or increasing Ru content, which indicates an increment in capacitance. Figure 9b shows the experimental specific capacitance (C_{sp}^{exp}) or total C_{sp}^{exp} contributed from both the GSs and RuO_2 in ROGSC electrodes and measured at 1 mV s^{-1} as a function of Ru loading. It can be found that the total C_{sp} shows a monotonic increment with increasing Ru loading of the composite. The pure GSs have a specific capacitance of 148 F g^{-1} and, for example, a specific capacitance of 570 F g^{-1} is obtained for the ROGSC electrode with 38.3 wt% Ru, which is

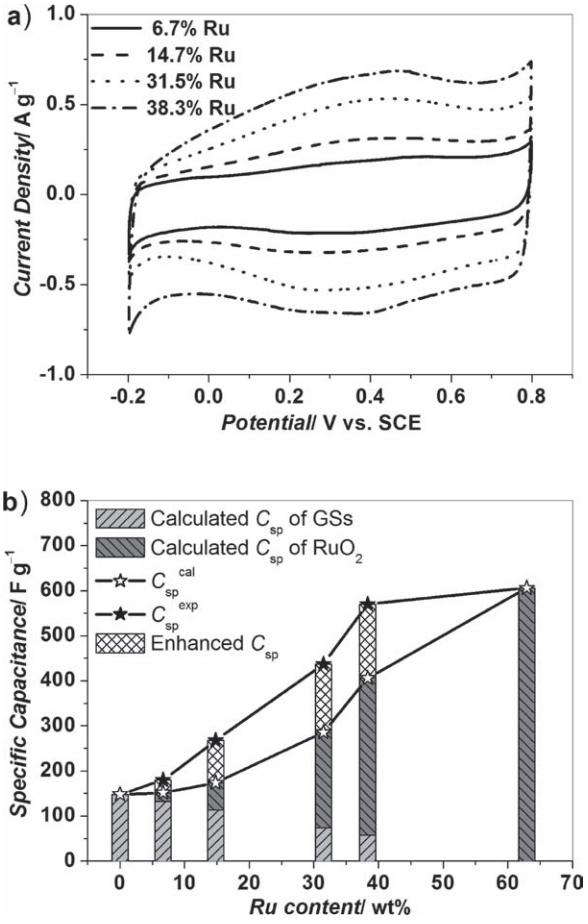

Figure 9. a) CV curves of ROGSC electrodes with different Ru content measured at 1 mV s^{-1}. b) Experimental and calculated specific capacitance of ROGSCs (C_{sp}^{exp} and C_{sp}^{cal}), the calculated C_{sp}^{cal} of ROGSCs is the sum of the calculated capacitances from GSs and RuO_2 components in ROGSCs. The intercrossed, slashed-line squares indicate the enhanced capacitances ($C_{sp}^{exp} - C_{sp}^{cal}$) due to the synergistic effects of GSs and RuO_2 in ROGSCs.

much higher than the corresponding values (basically less than 360 F g^{-1}) of other carbon/RuO_2 composites reported.[30,32–35,39] Moreover, it is important to note that the experimental total of ROGSCs is much higher than the calculated capacitance (C_{sp}^{cal}) of pure GSs as EDLCs (C_{sp}^{GS}, 148 F g^{-1}) and pure RuO_2 as pseudocapacitors ($C_{sp}^{RuO_2}$, 606 F g^{-1}) by a simple integration according to their weight ratios (Figure 9b), in terms of the equation: $C_{sp}^{cal} = C_{sp}^{RuO_2} \times \frac{Ru_{wt\%}}{62.9\%} + C_{sp}^{GS} \times (1 - \frac{Ru_{wt\%}}{62.9\%})$, where 62.9% is the weight ratio of Ru in $RuO_2 \cdot 1.53H_2O$.

The enhanced capacitance ($C_{sp}^{exp} - C_{sp}^{cal}$) strongly demonstrates the synergistic effects of GSs and RuO_2 to improve the electrochemical performance of ROGSCs (Figure 9b). On one hand, the loading of RuO_2 leads to the separation of neighboring GSs, and consequently results in rich porous texture and an enhanced available surface area for energy storage of EDLCs. On the other hand, the anchoring effect of separated GSs with the help of oxygen-containing functional groups enables the formation of well-dispersed fine RuO_2 NPs on GS surfaces and prohibits the agglomeration of fine RuO_2 NPs, which consequently ensures a better utilization of RuO_2. It has been reported that the electrochemical oxidation starts from the surface of RuO_2 particles, and only the surface region can be oxidized. Moreover, the oxidation rate becomes slower as the reaction proceeds from the surface to interior of the RuO_2 electrode.[31] Therefore, the well-dispersed small hydrous RuO_2 particles on GSs are easily and thoroughly electrochemically oxidized, and as a result, promote higher electrochemical capacitance. In summary, the great improvement in electrochemical capacitive performance of ROGSC electrodes is due to the unique particle–sheet structure, which allows the full utilization of the advantages of both GSs and RuO_2, and greatly decreases the interparticle resistance of electron pathways, reduces the diffusion path, and facilitates ionic motion during the charge-storage/delivery process.

2.3.3. Cycling Stability and Energy/Power Density

To evaluate the cycling stability and energy/power density of the as-prepared GS, RuO_2, and ROGSC (Ru, 38.3 wt%) electrodes, we carried out constant current charge–discharge tests using a cell-voltage window of 1 V in 1 M H_2SO_4 electrolyte. The cycling test was performed at a current density of 1 A g^{-1} for 1000 cycles. As shown in **Figure 10a**, the capacitance of the ROGSCs slowly decreases to 98.2% during the first 170 charge–discharge cycles, and then becomes quite stable. After

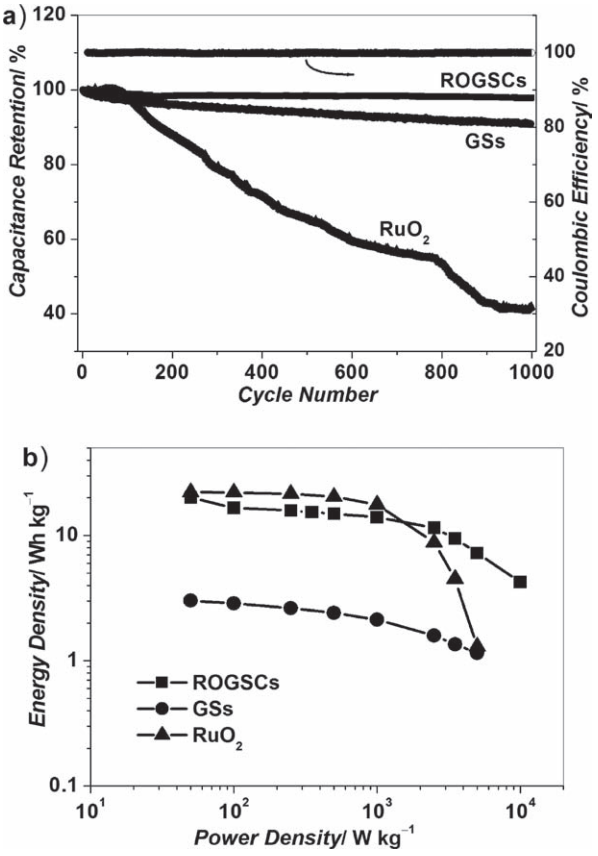

Figure 10. a) Cycling stability of the as-prepared GSs, RuO_2, and ROGSCs (Ru, 38.3 wt%) measured with a two-electrode cell at a current density of 1 A g^{-1} (Right: Coulombic efficiency of ROGSCs), and b) Ragone plot for the as-prepared GSs, RuO_2, and ROGSC (Ru, 38.3 wt%) supercapacitors.

the 1000th cycle, 97.9% of the original capacitance is retained, with a negligible capacitance loss of 2.1%. Compared with the capacitance of the pure RuO_2 electrode (~42.0%), GSs (90.9%), and other RuO_2/carbon composite electrodes, such as RuO_2/aligned carbon nanotubes (loss ~10%),[36] ROGSC electrodes show an improved cycling stability, which reveals their excellent electrochemical stability. The enhanced cycling stability of ROGSCs is due to the introduction of GSs in the composite, similar to the enhancements present in polyaniline/graphene[48] and SnO_2/graphene.[49] In addition, it is worth noting that the Coulombic efficiency of charge capacitance–discharge capacitance remains at almost 100% during the cycling process (Figure 10a). The Ragone plot of the as-prepared GS, RuO_2, and ROGSC (Ru, 38.3 wt%) supercapacitors illustrates the corresponding energy/power densities (Figure 10b), which were calculated from constant-current charge–discharge data at various current densities. The highest energy density obtained for ROGSCs is 20.1 Wh kg^{-1} while the corresponding power density is 50 W kg^{-1} (0.1 A g^{-1}). This value is slightly less than that of RuO_2 (22.2 Wh kg^{-1}), but much higher than that of GSs (3.1 Wh kg^{-1}). With increasing power density from 100 W kg^{-1} (0.2 A g^{-1}) to 1000 W kg^{-1} (2 A g^{-1}), the energy densities drop very slowly from 22.1 to 17.7 Wh kg^{-1} for RuO_2 and from 16.6 to 14.0 Wh kg^{-1} for ROGSCs. However, when the power density is larger than 1000 W kg^{-1}, the corresponding energy density of RuO_2 decreases rapidly and becomes 1.3 Wh kg^{-1} at 5000 W kg^{-1}. In contrast, ROGSCs still retain a high energy density of 7.2 Wh kg^{-1} at 5000 W kg^{-1} (10 A g^{-1}) and 4.3 Wh kg^{-1} at power densities as high as 10000 W kg^{-1} (20 A g^{-1}), thereby exhibiting the good power characteristic of ECs. The excellent electrochemical stability and high energy/power density of ROGSCs further demonstrate that the particle–sheet structure of ROGSCs plays an important role in facilitating ion transport and increasing energy storage during the charge-storage/delivery processes.

3. Conclusions

Hydrous RuO_2-anchored GSs for use as a composite electrode for supercapacitors were prepared by combining sol-gel synthesis and lower-temperature annealing. The GSs are well separated by tiny RuO_2 NPs with a size of 5–20 nm that act as spacers between neighboring GSs and the well-dispersed fine RuO_2 NPs are anchored on the surface of GSs with the help of oxygen-containing functional groups. The total C_{sp}^{exp} is greatly increased from 148 F g^{-1} for the as-prepared GSs to 570 F g^{-1} for the ROGSCs with 38.3 wt% Ru. Moreover, the total C_{sp}^{exp} of ROGSCs is higher than the simple sum of specific capacitances (C_{sp}^{cal}) of pure GSs and pure RuO_2 in their relative weight ratios. The increased specific capacitance ($C_{sp}^{exp} - C_{sp}^{cal}$) of ROGSCs demonstrates the positive synergistic effect of GSs and RuO_2 due to the utilization of the combined advantages of separated GSs to provide a large, accessible surface area, and a high conductive network of fine amorphous hydrous RuO_2 NPs. Furthermore, the ROGSC-based supercapacitors exhibit enhanced rate capability, excellent electrochemical stability (~97.9% after 1000 cycles), and high energy density (20.1 Wh kg^{-1}) or power density (10000 W kg^{-1}). Considering the full utilization of the advantages of GSs as EDLCs and RuO_2 as pseudocapacitors, we believe that the novel particle–sheet structured ROGSCs can be applied in high-performance energy-storage systems.

4. Experimental Section

Synthesis and Characterization of ROGSCs: The GSs used in this study were prepared by chemical exfoliation of natural graphite powder (500 mesh, Sinopharm Chemical Reagent Co., Ltd), as we reported elsewhere.[42] ROGSCs with different loadings of Ru were prepared by a sol-gel process and low-temperature annealing, similar to that previously used to prepare RuO_2.[29] Typically, the GSs obtained were firstly dispersed in a mixture of 1:1 (V:V) ethanol:water (100 mL), and stirred for 0.5 h. Then the given volume of $RuCl_3$ (0.1 M, Aldrich, USA) was added into the GS suspension and vigorously stirred for 0.5 h at room temperature. Subsequently, NaOH solution (1 M) was slowly added to adjust the pH to 7. The mixed solution was continuously stirred for 5 h, then filtered and washed with ethanol and water several times to remove residual chloride (NaCl), and finally dried at 60 °C in vacuum for 10 h and at 150 °C for 2 h. The loading amount of Ru in ROGSCs was controlled on the basis of the mass of $RuCl_3$ used with respect to the mass of GSs, and identified by EDS-equipped SEM. For comparison, hydrous RuO_2 was also prepared by the same procedure without the presence of graphene.

SEM characterization of the samples (GSs and ROGSCs) was performed using a FEI Nova Nano 430 system with an accelerating voltage of 15 kV, and the elemental composition (Ru, O, and C) of the samples imaged in SEM was identified by using EDS. TEM characterizations of ROGSCs were performed using a JEOL JEM 2010 TEM with an accelerating voltage of 200 kV. To make a TEM specimen, the as-prepared ROGSCs were first sonicated in ethanol (~0.02 mg mL^{-1}) for 5 min, and then a droplet of ROGSC dispersion was cast onto a TEM copper grid, followed by drying at room temperature. XPS measurements were performed on ESCALAB 250 with Al Ka radiation (15 kV, 150 W) under a pressure of 4×10^{-8} Pa. XRD measurements were conducted on a D-MAX/2400 with a Rigaku Multiflex powder diffractometer with Cu Ka radiation between 10° and 90° and an incident wavelength of 0.154056 nm. TGA/DTG measurements were carried out on Netzsch-STA 449C from 30 °C to 800 °C at a heating rate of 5 °C min^{-1} in air. Raman spectra were measured and collected using a 632.8 nm laser with JY HR800 under ambient conditions, with a laser spot size of about 1 μm. The specific surface area and porous parameters of GSs and ROGSCs were determined by using a Micromeritics ASAP 2010 M at 77 K. Before measurements, the samples were dried at 70 °C for 10 h in an oven, and then degassed at 150 °C for 12 h until the vacuum was less than 2 μmHg.

Preparation and Characterization of Supercapacitor Electrodes: The working electrodes of supercapacitors were fabricated as follows: active material (GSs, RuO_2, ROGSCs, 5 mg), carbon black (1 mg) as conducting adductive, and polytetrafluoroethylene (PTFE, 2.5 mg) were firstly mixed well in ethanol, and then pressed onto a Pt–Rh mesh which served as a current collector. The electrochemical performance of ROGSC electrodes was characterized by means of CV measurements and charge–discharge galvanostatic tests, with H_2SO_4 (1 M) as electrolyte. The CV measurements were carried out using a three-electrode cell, in which a platinum plate was used as counter-electrode and SCE as reference electrode, in the potential range of between –0.2 and 0.8 V vs. SCE with scan rates from 1 to 50 mV s^{-1}. The data was collected using an electrochemical workstation Solartron 1287. The charge–discharge galvanostatic tests of two-electrode cells were performed at current densities from 100 mA g^{-1} to 20 A g^{-1} using an Arbin BT 2000.

Supporting Information

Supporting Information is available from the Wiley Online Library or from the author.

Acknowledgements

This work was supported by the Ministry of Science and Technology of China (No. 2006CB932703), the National Science Foundation of China (No. 50872136, 50972147, 50921004, and 50632040), and the Chinese Academy of Sciences (No. KJCX2-YW-231). The authors acknowledge Mr. L.B. Gao and Z.P. Chen for valuable discussions.

Received: May 25, 2010
Published online: August 23, 2010

[1] P. Simon, Y. Gogotsi, *Nat. Mater.* **2008**, *7*, 845.
[2] C. Liu, F. Li, L. P. Ma, H. M. Cheng, *Adv. Mater.* **2010**, *22*, E28.
[3] M. Jayalakshmi, K. Balasubramanian, *Int. J. Electrochem. Sci.* **2008**, *3*, 1196.
[4] E. Frackowiak, F. Beguin, *Carbon* **2001**, *39*, 937.
[5] A. Burke, *J. Power Sources* **2000**, *91*, 37.
[6] E. Frackowiak, *Phys. Chem. Chem. Phys.* **2007**, *9*, 1774.
[7] D. W. Wang, F. Li, M. Liu, G. Q. Lu, H. M. Cheng, *Angew. Chem.Int. Ed.* **2008**, *47*, 373.
[8] K. H. An, W. S. Kim, Y. S. Park, J. M. Moon, D. J. Bae, S. C. Lim, Y. S. Lee, Y. H. Lee, *Adv. Funct. Mater.* **2001**, *11*, 387.
[9] J. P. Zheng, P. J. Cygan, T. R. Jow, *J. Electrochem. Soc.* **1995**, *142*, 2699.
[10] C. Ye, Z. M. Lin, S. Z. Hui, *J. Electrochem. Soc.* **2005**, *152*, A1272.
[11] Y. G. Wang, H. Q. Li, Y. Y. Xia, *Adv. Mater.* **2006**, *18*, 2619.
[12] B. E. Conway, W. G. Pell, *J. Solid State Electrochem.* **2003**, *7*, 637.
[13] K. H. An, K. K. Jeon, J. K. Heo, S. C. Lim, D. J. Bae, Y. H. Lee, *J. Electrochem. Soc.* **2002**, *149*, A1058.
[14] L. Z. Fan, Y. S. Hu, J. Maier, P. Adelhelm, B. Smarsly, M. Antonietti, *Adv. Funct. Mater.* **2007**, *17*, 3083.
[15] D. W. Wang, H. T. Fang, F. Li, Z. G. Chen, Q. S. Zhong, G. Q. Lu, H. M. Cheng, *Adv. Funct. Mater.* **2008**, *18*, 3787.
[16] K. S. Novoselov, A. K. Geim, S. V. Morozov, D. Jiang, Y. Zhang, S. V. Dubonos, I. V. Grigorieva, A. A. Firsov, *Science* **2004**, *306*, 666.
[17] A. K. Geim, K. S. Novoselov, *Nat. Mater.* **2007**, *6*, 183.
[18] A. K. Geim, *Science* **2009**, *324*, 1530.
[19] S. Park, R. S. Ruoff, *Nat. Nanotech.* **2009**, *4*, 217.
[20] S. Stankovich, D. A. Dikin, R. D. Piner, K. A. Kohlhaas, A. Kleinhammes, Y. Jia, Y. Wu, S. T. Nguyen, R. S. Ruoff, *Carbon* **2007**, *45*, 1558.
[21] H. C. Schniepp, J. L. Li, M. J. McAllister, H. Sai, M. Herrera-Alonso, D. H. Adamson, R. K. Prud'homme, R. Car, D. A. Saville, I. A. Aksay, *J. Phys. Chem. B* **2006**, *110*, 8535.
[22] Z. S. Wu, W. C. Ren, L. B. Gao, J. P. Zhao, Z. P. Chen, B. L. Liu, D. M. Tang, B. Yu, C. B. Jiang, H. M. Cheng, *ACS Nano* **2009**, *3*, 411.
[23] S. R. C. Vivekchand, C. S. Rout, K. S. Subrahmanyam, A. Govindaraj, C. N. R. Rao, *J. Chem. Sci.* **2008**, *120*, 9.
[24] M. D. Stoller, S. Park, Y. Zhu, J. An, R. S. Ruoff, *Nano Lett.* **2008**, *8*, 3498.
[25] H. L. Wang, Q. L. Hao, X. J. Yang, L. D. Lu, X. Wang, *Electrochem. Commun.* **2009**, *11*, 1158.
[26] D. W. Wang, F. Li, Z. S. Wu, W. Ren, H. M. Cheng, *Electrochem. Commun.* **2009**, *11*, 1729.
[27] Y. Wang, Z. Q. Shi, Y. Huang, Y. F. Ma, C. Y. Wang, M. M. Chen, Y. S. Chen, *J. Phys. Chem. C* **2009**, *113*, 13103.
[28] W. Lv, D. M. Tang, Y. B. He, C. H. You, Z. Q. Shi, X. C. Chen, C. M. Chen, P. X. Hou, C. Liu, Q. H. Yang, *ACS Nano* **2009**, *3*, 3730.
[29] C. C. Hu, W. C. Chen, K. H. Chang, *J. Electrochem. Soc.* **2004**, *151*, A281.
[30] Y. T. Kim, K. Tadai, T. Mitani, *J. Mater. Chem.* **2005**, *15*, 4914.
[31] H. F. Li, R. D. Wang, R. Cao, *Microporous Mesoporous Mater.* **2008**, *111*, 32.
[32] J. H. Jang, S. J. Han, T. Hyeon, S. A. Oh, *J. Power Sources* **2003**, *124*, 596.
[33] J. R. Zhang, D. C. Jiang, B. Chen, J. J. Zhu, L. P. Jiang, H. Q. Fang, *J. Electrochem. Soc.* **2001**, *148*, A1362.
[34] Y. F. Su, F. Wu, L. Y. Bao, Z. H. Yang, *New Carbon Mater.* **2007**, *22*, 53.
[35] X. F. Wang, D. Z. Wang, J. Liang, *Acta Phys. -Chim. Sin.* **2003**, *19*, 509.
[36] J. S. Ye, H. F. Cui, X. Liu, T. M. Lim, W. D. Zhang, F. S. Sheu, *Small* **2005**, *1*, 560.
[37] I. H. Kim, J. H. Kim, K. B. Kim, *Electrochem. Solid-State Lett.* **2005**, *8*, A369.
[38] G. Arabale, D. Wagh, M. Kulkarni, I. S. Mulla, S. P. Vernekar, K. Vijayamohanan, A. M. Rao, *Chem. Phys. Lett.* **2003**, *376*, 207.
[39] S. Mitra, K. S. Lokesh, S. Sampath, *J. Power Sources* **2008**, *185*, 1544.
[40] J. H. Park, O. O. Park, *J. Power Sources* **2002**, *109*, 121.
[41] P. V. Kamat, *J. Phys. Chem. Lett.* **2010**, *1*, 520.
[42] Z. S. Wu, W. Ren, L. Gao, B. Liu, C. Jiang, H. M. Cheng, *Carbon* **2009**, *47*, 493.
[43] H. L. Wang, J. T. Robinson, G. Diankov, H. J. Dai, *J. Am. Chem. Soc.* **2010**, *132*, 3270.
[44] G. X. Wang, J. Yang, J. Park, X. L. Gou, B. Wang, H. Liu, J. Yao, *J. Phys. Chem. C* **2008**, *112*, 8192.
[45] H. Kim, B. N. Popov, *J. Power Sources* **2002**, *104*, 52.
[46] K. N. Kudin, B. Ozbas, H. C. Schniepp, R. K. Prud'homme, I. A. Aksay, R. Car, *Nano Lett.* **2008**, *8*, 36.
[47] Y. C. Si, E. T. Samulski, *Chem. Mater.* **2008**, *20*, 6792.
[48] D. W. Wang, F. Li, J. Zhao, W. Ren, Z. G. Chen, J. Tan, Z. S. Wu, I. Gentle, G. Q. Lu, H. M. Cheng, *ACS Nano* **2009**, *3*, 1745.
[49] S. M. Paek, E. Yoo, I. Honma, *Nano Lett.* **2009**, *9*, 72.